eprints@whiterose.ac.uk
https://eprints.whiterose.ac.uk/

Twist-Bend Nematic Phase in Biphenylethane-based Copolyethers

Warren D. Stevenson [a,b], Jianggen An [a], Xiang-bing Zeng [b], Min Xue [a], Heng-xing Zou [a], Yong-song Liu [a], Goran Ungar [a,b,*]

[a] Department of Physics, Zhejiang Sci-Tech University, Hangzhou 310018, China
[b] Department of Materials Science and Engineering, University of Sheffield, Sheffield S1 3JD, UK

Abstract:

The main-chain liquid crystal (LC) copolyethers in which the nematic-nematic phase transition was first experimentally observed were revisited and re-characterised. Grazing incidence X-ray scattering revealed the low-T nematic (N_{tb} phase) could be highly aligned by shearing, more so than in previously studied bent LC dimers. This was evidenced by a four-point wide angle X-ray scattering pattern, which originates from convolution of two tilt distributions. Through intensity simulation the orientational order parameter associated with each of the distributions, as well as the conical angle of the N_{tb} phase, were calculated. Information regarding the polymer chain conformation was obtained using polarised infrared spectroscopy. The findings suggest the average conformation of the chains is a helix and that the bend angle between mesogenic units is inversely related to temperature. All experimental evidence, including a jump in birefringence at the N_{tb}-nematic (N) phase transition, shows that copolyether samples mirror the behaviour of bent LC dimers over the transition. This confirms the low-T nematic phase in copolyethers is indeed the same as that in LC dimers, now known to be the N_{tb}. The unusual broadening of transition peaks in complex heat capacity, obtained by modulated DSC experiments, is discussed.

Keywords: nematic-nematic transition; N_{tb} phase; liquid crystal; main-chain polymer; X-ray scattering; polarized infrared; liquid crystal dimer.

Introduction

Historically, the first experimental observations of the nematic-nematic phase transition were reported in early 1990's in a series of main-chain liquid crystal (LC) copolyethers featuring semi-flexible biphenylethane (BPE) mesogens, linked by odd-numbered oligomethylene spacers.[1-3] The transition was not observed in polymers with even spacers, indicating the bend between successive mesogens, imposed by odd spacers, was key to observing the transition. Partial flexibility of BPE mesogens was also deemed important since no other odd spacer polymers exhibited the transition. By DSC the transition appeared as a sharp, highly reversible endo/exotherm on heating/cooling. X-ray Bragg reflections were not observed either side of the DSC peak, signalling lack of long range positional order in both phases. However in well oriented polymer fibres, significant changes were observed in both radial and azimuthal wide angle X-ray scattering (WAXS) intensity: the Low-T phase produced a characteristic four point WAXS pattern[2] with larger reciprocal spacings. This revealed closer packing and a more complex local structure in the Low-T phase.

In recent times the nematic-nematic transition is one of the hottest topics in LC research and is now additionally observed in LC bent core molecules,[4] trimers,[5-8] tetramers,[9,10] hexamers[10] and dimers. The latter, comprising rigid aromatic mesogens and odd oligomethylene spacers,[11-28] are the most frequently studied. The low-T nematic, previously labelled "n2",[1] but commonly named twist bend nematic (N_{tb}), is now known to exhibit spontaneous mirror symmetry breaking, despite its chemically achiral constituents. Contrary to cholesteric phases, mesogens in the N_{tb} phase tilt at an angle $\neq 90°$ to the helical axis and complete the pitch in a few molecular lengths. A nano-scale heliconical pitch length ranging between 8 and 12 nm was confirmed by resonant X-ray scattering[11-13] and coexistence of oppositely handed domains has been demonstrated by NMR[14-16] and optical microscopy.[17-20] Topographic methods such as AFM[21] and cryo-TEM[22,23] have also suggested a helical pitch length of 8-10 nm.

In light of recent advances in subject knowledge, we revisit the nematic phases and their transition in main-chain copolyethers. Importantly, all experimental findings in copolyethers bear close resemblance to those reported in bent LC dimers, leaving little doubt that the low-T nematic phase is identical in both types of systems. Thus, in the following we refer to the low-T phase in copolyethers as N_{tb}. Further to previous work on copolyethers, optical birefringence, polarized optical micrographs (POM), modulated DSC (MDSC), grazing incidence X-ray diffraction (GIXRD) and polarized IR spectroscopy were recorded over the range of the two nematic phases. We obtained the average tilt or 'conical angle' in the N_{tb} phase, the conical distribution and the deconvoluted domain order parameter, which was found to be as high as 0.9. The first polarized IR and MDSC studies on the N_{tb} phase provide new information on orientational and conformational order, and suggest molecular weight separation at the transition.

Materials

The two nematic phases were re-investigated in two previously studied main-chain copolyethers, comprising semiflexible BPE-based mesogens linked by -O(CH$_2$)$_{5,7}$O- (Copolymer) or -O(CH$_2$)$_{5,7,9}$O- spacers (Terpolymer). In Copolymer and Terpolymer the odd spacers are present in molar ratios of 1:1 and 1:1:1, respectively and are randomly distributed along the chain (Figure 1a). As found previously,[2] copolymerization suppresses crystallisation, rendering both nematics thermodynamically stable and amenable to further studies. In addition to mixed spacers, two differently substituted BPE mesogens (methyl or chloro group) are randomly distributed in a 1:1 molar ratio (Figure 1a). The synthesis of Copolymer and Terpolymer is based on that in refs. 1,2 and 29, and is described in the Supporting Information (SI). Based on GPC the molecular weight and polydispersity of Copolymer are M_w = 26,724 and M_w/M_n = 1.63, while for Terpolymer M_w = 26,897 and M_w/M_n = 1.52.

Conventional DSC

Conventional DSC measurements were performed using a TA Instruments Q2000 DSC fitted with a cooling unit and a TZero high sensitivity cell. The heating and cooling traces of Terpolymer are shown in Figure 1b, while those of Copolymer are shown in Figure S5 (SI). The phase assignments were confirmed by GIXRD experiments, which are discussed further below. Upon cooling (1 K/min) from the isotropic (Iso) liquid, as well as on subsequent heating, both polymers exhibited only the N and N$_{tb}$ phases. Incidentally, T$_{Ntb-N}$ and T$_{N-I}$ of the polymers coincide with the linear relationship derived for two ring dimers/bimesogens by Mandle et al.[30,31] After standing at 20 °C for 6 hours, Copolymer developed ≈1% crystallinity, indicated by a small endotherm near 80 °C. No crystallization was observed in Terpolymer even after ≈120 hours standing – see Figure S6 (SI). It was thus decided to carry out further experiments on Terpolymer.

Optical Microscopy and Birefringence

Terpolymer was investigated using an Olympus BX50 microscope fitted with a Mettler FP82 HT hotstage. Uniform films were prepared by drop-casting from dichloromethane solution. Upon 0.1 K/min cooling from the Iso to N phase, a grainy first order birefringent texture developed. This texture is common in both nematic and smectic main-chain LC polymers.[32] With continuous cooling into the N$_{tb}$ phase, the texture did not change noticeably and remained fine and grainy even after annealing at 50 °C for ≈120 hours (Figure 1c). With a λ-plate, the top-left and bottom-right quadrants of 1c are mostly blue, while the other two are mostly yellow, similar in appearance to strength ±1 disclinations. The film was then sheared in the N$_{tb}$ phase, obtaining Figure 1d. The stripes ran mostly perpendicular to the shearing direction, suggestive of the "banded texture".[32,33] The banded texture has been observed in a wide range of thermotropic
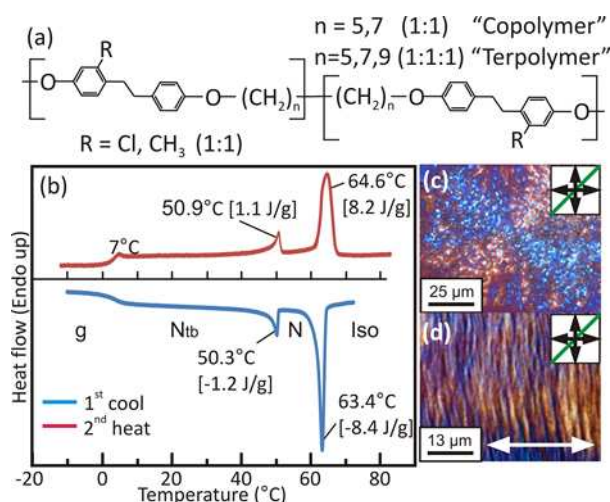

Figure 1 – (a) Chemical composition of BPE copolymers. (b) DSC curves of Terpolymer. The rate was 1 k/min in all cases. Transition Enthalpy in square brackets. (c) Grainy texture observed after annealing Terpolymer in the N phase for ≈120 hours at 50 °C. (d) "Banded" texture achieved after shearing Terpolymer in the N$_{tb}$ phase between glass plates at RT. Shear direction is indicated by arrows. Green indicates axis of λ-plate.

LC polymers and is explained by relaxation (elastic contraction) of the chains in response to rapid flow (shearing). This produces a periodically undulating director along the direction of flow.[32,33] Much smaller regions of banding were observed after shearing in the N phase, implying that the stripes do not correspond to the rope-like N$_{tb}$ texture observed in LC dimers.

A new Terpolymer sample was prepared by directly melting onto a glass plate (Iso phase), cooling to room temperature (RT) and shearing vigorously using a scalpel blade. High sample alignment was achieved (Figure S7c). With shear direction northwest to southeast and with the λ-plate inserted, the texture was bright first order yellow, suggesting the polymer chains were oriented along the shear direction.

Birefringence (Δn) of the shear-aligned Terpolymer film was investigated using a Berek compensator. The film thickness in the region of retardation measurements was determined from 3D sample profiling (see SI). At RT (N$_{tb}$ phase) Δn of Terpolymer was 0.027±0.003. The sheared film was heated at a rate of 0.5 °C/min into the Iso phase. The temperature dependence of Δn is shown in Figure 3d. In the N$_{tb}$ phase Δn was found to slowly increase linearly with temperature. At the N$_{tb}$-N transition a small but distinct and

reproducible jump was observed. On further heating this was followed by a slow, then rapid drop in Δn toward the N-Iso transition. Similar behaviour has been reported in bent LC dimers.[17,23]

GIXRD Analysis

GIXRD experiments were performed on beamline BM28 of the ESRF. Terpolymer on a silicon substrate was heated to 100 °C, cooled to RT (N_{tb}) and sheared by scalpel. The sample was then placed on the temperature controlled surface of a custom six-circle goniometer with shear direction perpendicular to incident beam. A helium-filled flight tube was positioned between the sample and a Mar165 CCD detector.

At RT (23 °C) the GIXRD pattern of the sheared N_{tb} phase (Figure 2a) exhibited no small angle features, only broad WAXS centered at q=14.6 nm^{-1} (d=0.43 nm), arising from lateral chain packing. Unlike observations in LC dimers, the WAXS had four intensity maxima rather than just two azimuthally broadened arcs. Note only half of the pattern is visible in Figure 2a-d due to the grazing incidence geometry. Four WAXS maxima in the N_{tb} phase were observed in earlier work on oriented BPE-type copolymer fibres.[2] As the temperature was incrementally raised from RT, the WAXS intensity distribution progressively changed from four maxima in the N_{tb} phase to two equatorial maxima (d=0.45 nm) in the N phase (Figure 2b). Sample orientation was lost close to T_{N-Iso} (Figure 2c). To test the reversibility of the azimuthal intensity shifts, Terpolymer was re-sheared at RT and incrementally heated to 55 °C (N phase); the sample was then cooled back into the N_{tb} phase (Figure 2d). The progressive changes in the azimuthal WAXS distribution during this heating/cooling process are shown in Figure 2e. 90 ° corresponds to the equator, while 0 and 180 ° correspond to the meridian and fibre axis. When re-cooled into the N_{tb} phase the WAXS pattern remained as two equatorial arcs, but broader than in the N phase. Thus orientational order did not recover to its starting point.

To correct for Ewald sphere curvature in reciprocal space, the measured azimuthal angle (γ) was converted to 'polar angle' (Ψ) by $\cos(\Psi)=\cos(\gamma)\cos(\beta)$ (2β=scattering angle – see geometry in Figure S10). The intensity scattered by the N_{tb} phase in reciprocal space was then reconstructed using Equation 1:

$$I(\Psi) = \int_{0}^{90} \int_{90-\Psi}^{90} \frac{I(\theta_t,\Omega)\sin(\theta_t)}{\sqrt{\sin^2(\Psi)-\cos^2(\theta_t)}} \, d\,\theta_t d\Omega \quad (1)$$

A more basic form of Equation 1 is derived elsewhere in the context of conventional nematic phases,[34] i.e. a cylindrically averaged distribution of rod-like units around the director/axis of rotation. However, in the N_{tb} phase the conventional nematic director becomes the helical axis and the units preferentially tilt by an angle θ_t with respect to it. This means that the tilt distribution of the units, $D(\theta_t)$, is not centred on $\theta_t = 0$ (see inset of Figure 2f). Moreover
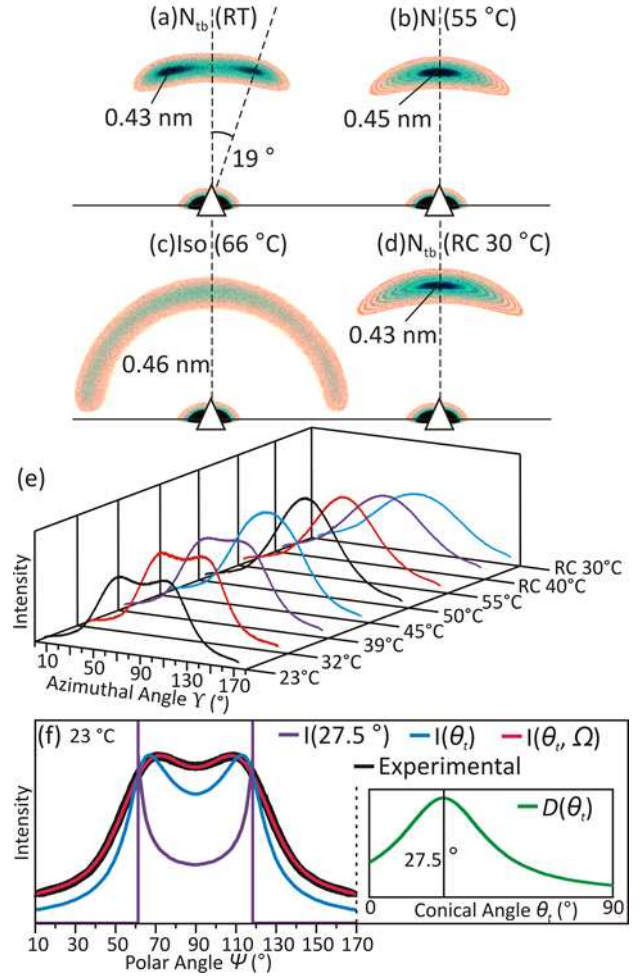

Figure 2 – GIXRD patterns of Terpolymer: (a) N_{tb} phase after shearing at RT. (b) Heated into N phase. (c) Heated to Iso phase. (d) Re-cooled (RC) to 30 °C from N phase (55 °C). Vertical dashed line is the equator and the solid horizontal line is the fibre (shear) axis and meridian. (e) Azimuthal intensity plots. (f) Fitting of the polar corrected intensity distribution at 23 °C. Curves are shown for a fixed conical angle (I(27.5 °)), a conical angle distribution ($I(\theta_t)$) and distributions of both conical angle and helical axis ($I(\theta_t, \Omega)$). Inset shows the real space conical distribution, $D(\theta_t)$, used to obtain the fit to the experimental data.

the helical axis in the N_{tb} phase is not fixed between domains and so an angular distribution of rotational axes, $D(\Omega)$, must also be considered. $I(\theta_t,\Omega)$ is thus the wide angle intensity scattered in reciprocal space by a convolution of both real space distributions, $D(\theta_t) \otimes D(\Omega)$.

A mathematically modelled 1D intensity profile was fitted to the polar corrected experimental line-shape by varying θ_t, the shape of $D(\theta_t)$, the shape of $D(\Omega)$ and their FWHMs, $\Delta\theta_t$ and $\Delta\Omega$, respectively. The fitting was tried exclusively with Gaussian distributions, exclusively with Lorentzian distributions and with combinations of the two, but best fit (Figure 2f) was obtained with Gaussians in both θ_t and Ω, with parameters θ_t=27.5 °, $\Delta\theta_t$=19 ° and $\Delta\Omega$=21°. Using these parameters one can determine the

degree of orientational order in the N_{tb} phase, which to date has been investigated by optical birefringence,[17,23] Raman scattering,[35] X-ray scattering[12,36] and NMR spectroscopy.[16,37] However, in these previous studies orientational order is quantified using $S=\langle P_2(\cos(\theta))\rangle = \langle(3\cos^2(\theta)-1)/2\rangle$. Treatments such as this typically result in $S=0.4$-0.6 in well aligned N_{tb} phases[16,35,37] because $\langle P_2\rangle$ is fundamentally limited to values $\ll 1$. This is due to $\theta_t \gg 0$. The tilt angle is often considered,[35,37] but all previous treatments assume the helical axis is constant, which is unrealistic. It has been shown by resonant X-ray scattering[12] that coherent helical N_{tb} domains can have dimensions on the scale of 0.1 µm, much smaller than the cross-sectional area of any instrumental sampling size. If experimental measurements sample several domains, a distribution of rotational axis directions must be accounted for. It was proposed in ref. 12 that orientational order in the N_{tb} phase would be better described using a two part orientational order parameter $S=S_0 \cdot S_1$, where S_0 describes the orientational order among helical domains and S_1 the tilt distribution of molecules inside each domain. This notion will be continued here because two distributions are indeed required to fit our N_{tb} azimuthal WAXS profile. If each domain is defined by a single rotational axis, S_0 and S_1 can be directly related to the rotational axis distribution, $D(\Omega)$, and molecular tilt distribution, $D(\theta_t)$, using equations 2 and 3, respectively:[38]

$$S_0 = \frac{\int_0^{90} D(\Omega)\langle P_2\rangle \sin(\Omega)\,d\Omega}{\int_0^{90} D(\Omega)\sin(\Omega)\,d\Omega} \qquad (2)$$

$$S_1 = \frac{\int_0^{90} D(\theta_t)\langle P_2\rangle \sin(\theta_t)\,d\theta_t}{\int_0^{90} D(\theta_t)\sin(\theta_t)\,d\theta_t} \qquad (3)$$

Using values obtained from WAXS fitting, the N_{tb} four point scattering pattern corresponds to $S_0=0.93$ and $S_1=0.62$. The order parameter measurable by experimental means would therefore be $S=S_0 \cdot S_1=0.58$, in line with values often reported for the N_{tb} phases of bent LC dimers, $S=0.4$-0.6.[16,35,37] An average tilt or 'conical angle' of 27.5 ° is in close agreement with current measurements.[12,17] In the N phase a suitable fit to the polar corrected data was obtained without complicated mathematical modelling using a Gaussian peak centred on the equator. We estimate $S = 0.68$ based on FWHM/2 of the fitted Gaussian. Re-cooling through the N-N_{tb} transition, the radial position of the peak shifted back to higher q ($d = 0.43$ nm), consistent with previous reports.[1] The intensity maximum remained centred on the equator after the transition, but spread to wider azimuthal angles. The spread is thought to be loss of orientation, i.e. lowering of S_0, rather than a change in mesogen tilt angle, θ_t. An increased azimuthal spread after the N-N_{tb} transition is also observed by X-ray scattering in magnetically aligned samples of bent LC dimers.[14,23,36] This further supports that the transition is the same in both sample types. The absence of the four-point N_{tb} WAXS pattern in LC dimers may be due to the much lower S_0.

Polarised IR Analysis

Terpolymer was deposited directly onto KBr, heated into the Iso phase, cooled to RT and sheared by scalpel. Linearly polarised infrared (IR) spectra were recorded using a Nicolet iS50 FTIR spectrometer with a temperature controlled cell and a ZnSe polariser. IR spectra were recorded with the polarity of incident radiation running parallel and perpendicular to the shear direction, and every 15 ° in between. This process was carried out at 25 °C and repeated in 5 °C increments up to 65 °C. Representative spectra of Terpolymer at 25 °C, with shear direction at 0, 45 and 90 ° to incident beam polarity are shown in Figure 3a. The wavenumbers of prominent peaks are provided in Figure 3b with proposed assignments. The assignments follow a previous non-polarized IR study by Silvestri and Koenig[39].

Orientational order parameter (S) of each vibrational mode was estimated using $S=(K-1)/(K+2)$,[40] where $K=A_{//}/A_{\perp}$ is the dichroic ratio (A is IR absorbance). To improve accuracy of 'K' values, the amplitude of each peak was plotted against sample orientation angle and a $\cos^2$ curve was fitted to the data (example in Figure S11 SI). The peak and trough of the fitted sinusoid were taken as $A_{//}$ and $A_{\perp}$. This data reduction process was repeated for spectra in each 5 °C increment, enabling S of each vibrational mode to be plotted against temperature. S curves for the vibrational modes of interest are shown in Figure 3c. In the N_{tb} phase, $S(T)$ is almost constant for all IR modes, but on transition to N phase, an abrupt bump or dip appears for several bands. A sudden change at the N_{tb}-N transition was similarly observed in birefringence (Figure 3d), although IR suggests orientational order decreases more rapidly with temperature in the N phase. Highest S values are in line with those estimated by our X-ray intensity model and also with measurements made elsewhere in the N_{tb} phase.[16,35,37] Positive S indicates vibrational modes oscillating below the 'magic angle' ($\simeq 55°$), while negative S indicates modes that oscillate at larger angles (in reference to the shear direction).
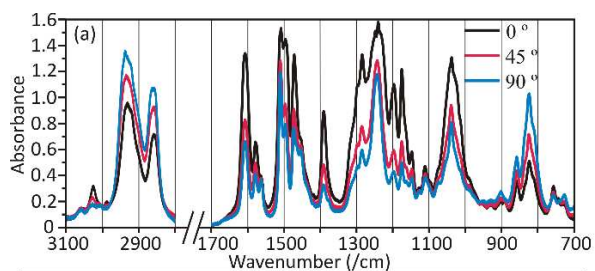
| IR Peak (cm⁻¹)	Peak Assignment (b)	S (@ 25 °C)	θ_v (°)
■ 1392	Wagging of CH$_2$ in OM spacer	0.53	28
▲ 1200	C-C stretching in dimethylene	0.48	31
◆ 1176	C-C stretching in dimethylene	0.41	34
■ 756	Rocking of CH$_2$ in dimethylene	0.27	42
■ 3030	C-H stretching in Ph	0.25	42
● 1039	Ph-O (C-O-C) symmetric stretching	0.23	44
◆ 1475	Scissoring of CH$_2$	0.21	44
● 1244	Ph-O (C-O-C) asymmetric stretching	0.10	50
■ 1111	CH$_2$-O (C-O-C) asymmetric streching	0.08	51
● 2931	Alkyl C-H stretching	-0.12	61
▲ 858	C-H OOP deformation (1,2,4 Ph)	-0.13	62
▲ 2864	Alkyl C-H stretching	-0.14	62
● 725	Rocking of CH$_2$ in OM spacer	-0.21	67
◆ 823	C-H OOP deformation (para Ph)	-0.23	68
1610	C-C stretching in Ph rings	0.28	41
1581	C-C stretching in Ph rings	-	-
1566	C-C stretching in Ph rings	-	-
1512	C-C stretching in Ph rings	0.08	51
1498	C-C stretching in Ph rings	-	-
1456	C-C stretching in Ph rings	-	-
1149	Uknown	-	-
1128	Uknown	-	-
903	Uknown	-	-
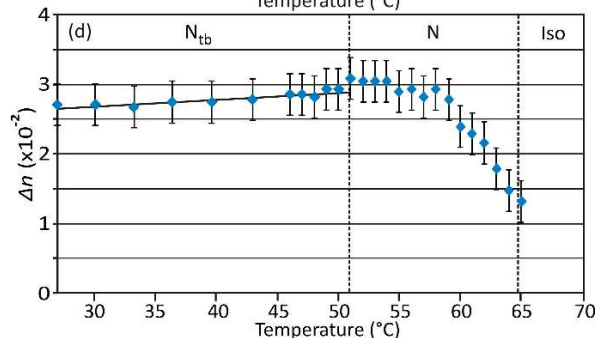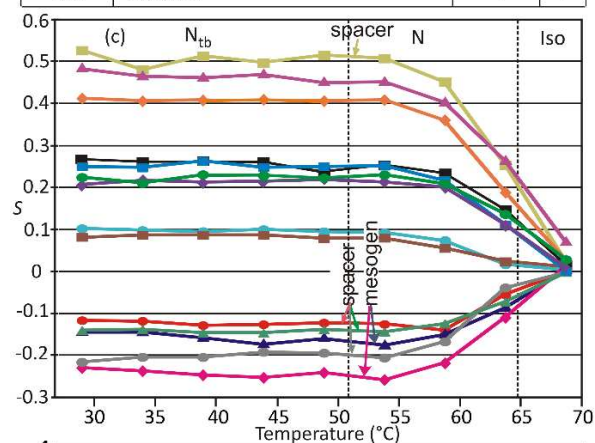
Figure 3 – (a) Polarised IR spectra of Terpolymer after shearing in the N$_{tb}$ phase at RT. Spectra are shown with the IR polarisation parallel (0 °, black), perpendicular (90 °, blue) and at 45 ° (red) to shearing direction. (b) Band assignment after ref. 39. The bands measured are listed first in order of descending S. OM = Oligomethylene (i.e. C$_5$H$_{10}$, C$_7$H$_{14}$ or C$_9$H$_{18}$), Ph = Phenyl, OOP = Out of Plane. Experimental vibration angles (θ_v) were calculated from S_1 = S/S_0 = (3cos^2(θ_v)-1)/2, where S_0 = 0.79 at 25 °C. (c) Temperature dependence of the orientational order parameter (S) calculated from IR dichroism. (d) Optical birefringence (Δn) of Terpolymer with increasing temperature.

The measured value of S can be described by the product of two order parameters S_0 and S_1; however in the context of IR modes, S_1 describes the tilt distribution of a particular bond type rather than whole polymeric units. To extract the two parameters from IR data, several rationalisations were made: (i) The transition moment of the CH$_2$ wagging mode in OM spacers (1392 cm⁻¹) is perpendicular to that of the CH$_2$ stretching (2931, 2864 cm⁻¹) and rocking (725 cm⁻¹) modes. (ii) The CH$_2$ wagging mode (1392 cm⁻¹) has the highest measured value of S, indicating that the transition moment is almost aligned with the chain axis, i.e. the angle of vibration θ_v must be close to the average N$_{tb}$ conical angle θ_t. (iii) The same value of S_0 applies to all modes, meaning that only S_1=<P$_2$(cos(θ_v))> is bond specific. A model was constructed where θ_v of the 1392 cm⁻¹ CH$_2$ wagging mode was varied, enabling a trial value of S_0 to be calculated by S/S_1. Using the trial value of S_0, S_1 and the corresponding value of θ_v were obtained for each remaining vibrational mode. The correct value of S_0 was deemed the value that produced CH$_2$ stretching and rocking modes oriented nearly 90 ° to CH$_2$ wagging modes. This was best achieved for S_0= 0.79. Note that only the magnitude of θ_v was determinable due to the cos^2 function (|28-90|=62 °). This value of S_0 (0.79) is smaller than that suggested by our X-ray intensity model (0.93), but this is unsurprising because the polymer could not be sheared as vigorously on the soft KBr surface as on the harder silicon one. We expect that sample alignment may have been poorer on the KBr substrate.

From estimated θ_v, details about the average polymer chain conformation can be ascertained. For example, the C-C stretching modes in the dimethylene group in the middle of the BPE mesogen (1200, 1176 cm⁻¹) vibrate at a similar angle to the CH$_2$ wagging modes in the OM spacer, which is close to the conical angle of the N$_{tb}$ phase (27.5 °). This suggests that the average conformation of the chains is a continuous helix, i.e. the mesogens and OM spacers tilt at approximately the same

angle with respect to the helical axis. The alternative interpretation is stretched chains tilted at a high angle (of the order of 45 °) to the shear axis, but this is highly unlikely and not seen in any other LC system. An average helical conformation has been proposed in earlier reports on the N_{tb} phase[9] including our own study of the mixture known as 'Se45'.[12] We note that C-C stretching modes at 1200 and 1176 cm^{-1} were assigned only tentatively in previous work,[39] but accepted here because high mesogen alignment and low conformational variety in short BPE spacers, hence high S, are sensible.

A BPE polymer chain segment was constructed in Material Studio (Accelrys) without torsional energy minimisation. From the 'all trans' conformation shown in Figure 4a the average length of the monomer units in BPE polyethers was estimated as 2.17 nm, thus a projected height of 2.17cos(27.5)=1.92 nm along the N_{tb} helical axis. This is comparable to the projected inter-mesogen separation in a dimer sample known as "Se45" (1.99 nm). The N_{tb} conical angle of Terpolymer (27.5 °) is also close to that of Se45 (29 °). Based on the closeness of these length scales and tilt angles, we predict the pitch length (p) is approximately the same in both samples. In Se45 p=10 nm at low-T, which is a commonly reported value in other samples.[11,19,22] Assuming a 10 nm pitch length and a conical angle of 27.5 ° we estimate that each Terpolymer unit contributes α=69 ° ($2\pi(1.92)/10$) of rotation around the helical axis. The average exterior angle between two conjoined mesogens can then be estimated as ϕ=30.4° ($\sin(\phi/2)=\sin(\theta_t)\sin(\alpha/2)$). In the 'all trans' conformation the BPE mesogens are mirrored about the central CH$_2$ unit of the OM spacer. However, when the chain is tilted by 27.5 ° to the helical axis, the exterior bend angle ϕ brings one mesogen closer to parallel with the helical axis than the other (Figure 4a). In order to obtain high order parameters for dimethylene C-C stretching modes, the angle to the helical axis must be similar for all mesogens. This can only be achieved if the polymer chain segments twist in a chiral conformation (example in Figure 4b). Due to flexibility of the mesogens and OM spacers, as well as rotational freedom about the oxygen bonds, there are many twisted conformations that can achieve the same bend angle; thus a specific twist angle cannot be quantified. A more complex conformational study, such as that for dimeric materials,[41] is the subject of future investigation.

At risk of over interpreting Figure 3c, we note subtle differences in the behaviour of mesogen and spacer bands at the N_{tb}-N transition, in particular concerning bands with highest and lowest S, which are most sensitive to orientational change. At low S the mesogen bands at 858 and 823 cm^{-1} show a small increase in orientation at 51 °C (S more negative), while S of the CH$_2$ (C-H) vibrations at 725, 2864 and 2931 cm^{-1} remain almost unchanged. At high S, the S-value for the 1392 cm^{-1} OM spacer band decreases between 49 °C and 54 °C, while the two mesogen bands at 1200 and 1176 cm^{-1} do not change.
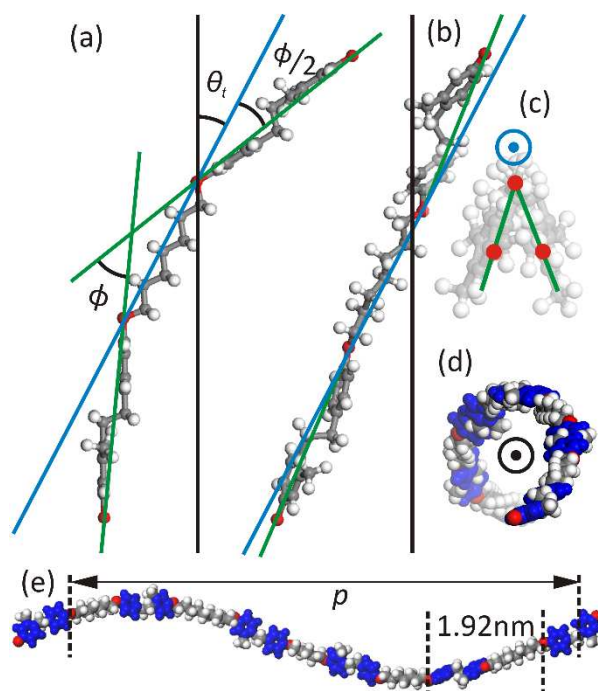

Figure 4 –MBPE homopolymer chain segment (methyl sub. units) with OM spacer axis tilted at θ_t = 27.5 °. (a) 'All trans' conformation. The axes of the OM spacer (blue) and DPE mesogens (green) are defined by oxygen atoms (red). The bend angle ϕ and the angle between the mesogen and spacer axes ($\phi/2$) are also defined. (b) Example twisted conformation with $\phi/2$ = 15.2 °. Torsion angles have been manually adjusted for illustration purposes. Helical axis (black) vertical. (c) Views of twisted conformation along OM spacer axis. (d) MBPE chain section showing a full helical rotation along the helical axis. (e) View of the chain from the side showing the pitch length (estimated as 10 nm) and the average monomer length.

Constant S so close to T$_{N-I}$ must mean an effective increase in S_1. Although the differences between mesogen and spacer bands may be at the limit of experimental error, their consistency suggests a reduction in the bend angle between mesogens, i.e. partial straightening of the chains at the N_{tb}-N transition.

Modulated DSC

The characteristics of the phase transition were investigated in Terpolymer by MDSC using the Q2000 instrument. In MDSC experiments a sinusoidal modulation of amplitude ΔT_M is superimposed on a slowly and linearly increasing or decreasing temperature to give

$$T(t) = T_0 + vt + \Delta T_M \sin(\omega t) \qquad (4)$$

where T_0 is the starting temperature, v the linear heating or cooling rate and ω the angular frequency of the modulation. Heat flow $Q_M(t)$ above that caused by the linear increase in temperature is

$$Q_M(t) = Q_{M,0}\cos(\omega t\text{-}\phi) \qquad (5)$$

where $Q_{M,0}$ is the amplitude and ϕ the phase shift between the temperature modulation and the responding heat flow. The complex heat capacity is thus

$$C_p{}^*(\omega) = \left(Q_{M,0}\big/\Delta T_M\omega\right)e^{i\phi} \qquad (6)$$

and its real (storage) component

$$C_p{}'(\omega) = \left(Q_{M,0}\big/\Delta T_M\omega\right)\cos\phi \qquad (7)$$

In our experiment v = 0.04 K/min, ΔT_M = 0.07 K and ω = 0.31 rad/s (period = 20 s). Figure 5 shows the phase angle $\phi(T)$ and the in-phase heat capacity $C_p'(T)$ for Terpolymer in the N_{tb}-N and N-Iso transition regions. The conventional DSC heat flow (Q_L) is also shown. A non-zero ϕ indicates lagging thermal response of the sample. The appearance of a peak in phase $\phi(T)$ indicates a first order phase transition.[42] Following this criterion, both the N_{tb}-N and N-Iso transitions in Terpolymer are first order.

There are two notable differences between the conventional DSC and MDSC curves in Figure 5. (1) The size of the N_{tb}-N peak relative to that of the N-Iso peak is larger in $C_p'(T)$ than in conventional $Q_L(T)$. This may be attributed to the N-Iso peak containing a larger "non-reversing" component that is subtracted when determining C_p^*. (2) More importantly, the MDSC peaks, recorded during very slow heating (0.04 K/min), are significantly broader than those recorded in the faster conventional DSC scan (1 K/min). This is opposite to the behaviour of small molecules where transition peaks become sharper at slower rates.[42,44] We speculate that MDSC peak broadening in the polymer comes from molecular weight (MW) segregation, whereby near-equilibrium partition between phases is maintained at any temperature during the slow T scan. Notably e.g. the tail of the N-Iso peak extends to 80 °C in $\phi(T)$, while in $Q_L(T)$ it ends at 68 °C. Thus the N-Iso transition in the MDSC experiment continues well beyond the peak temperature, presumably in segregated areas of higher MW. It is well known that T_{N-I} is strongly dependent on the MW of a polymer.[32] In the faster $Q_L(T)$ scan, segregation has no time to take place and the transition happens simultaneously in the uniformly mixed sample.

There is also a conspicuous difference between the asymmetric shape of the N_{tb}-N peak, which has a remarkably sharp high-T cut-off, and the symmetrically broadened profile of the N-I peak. This suggests that islands of N_{tb} phase cannot exist in an N phase matrix (above T_{Ntb-N}) in the way that islands of N phase can exist in an Iso matrix (above T_{N-Iso}). The high dependence of T_{N-I} on MW and the apparent low dependence of T_{Ntb-N} points to a crucial difference between the two transitions in main-chain polymers. The N-Iso transition involves a major change in overall chain conformation, from largely

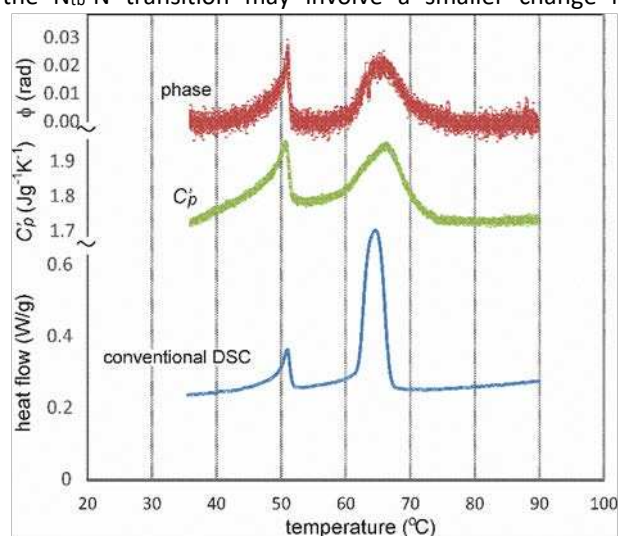extended in N-phase to random coil in Iso.[45] In contrast, the N_{tb}-N transition may involve a smaller change in

Figure 5 – MDSC heating traces for Terpolymer. Top: phase angle ϕ corrected for thermal lag in the pan and the sample assembly.[43] Middle: real component of complex heat capacity. Bottom: heat flow in conventional DSC experiment at 1 K/min, for comparison.

macro-conformation, hence no MW dependence. The MW effect on T_{Ntb-N} is the subject of further investigation.

Discussion

In the N_{tb} phase of Terpolymer, polarised IR spectroscopy suggests a twisted chain conformation. The small angle between the average spacer and mesogen axes infers that the chains select an average conformation resembling a continuous helix (Figure 4), in-line with a previous model proposed for bent LC dimers.[9,12] However, a dimer presents a short segment of a helix, while the average polymer chain studied here, containing 81 monomer units, presents a helix 156 nm in length (1.92*81), i.e. ≈15 pitch lengths (if no folds are present). Peak fitting of the GIXRD azimuthal intensity profile indicates that the average tilt, or 'conical angle', of the chains in the N_{tb} phase, is θ_t = 27.5°, in-line with that reported for bent LC dimers.[12,17] The merger of the diffuse WAXS doublet to singular equatorial peak close to T_{Ntb-N}, and the simultaneous increase in birefringence with a jump at T_{Ntb-N}, are consistent with straightening of the chain, i.e. a progressively reducing bend angle with increasing temperature. The conical angle may also change slightly with temperature; the calculated orientational order parameters (S) of some mesogen-related IR modes show hints of an increase.

Finally, it is appropriate to ask why so far only this unconventional series of polymers, with semi-flexible mesogens, exhibit the N_{tb} phase, when so many other main-chain polymers with rigid mesogens and odd spacers do not. We can think of two possible reasons: (1) The flexibility of the mesogens helps the chain adopt a smooth helical conformation required by the N_{tb} phase. (2) Relative to the smectic or crystal phase, the N_{tb} phase is

stabilized by the entropy of longitudinal motion, enabled by a helical director field. Consider that the barrier for longitudinal motion includes a term E_0^* for an aromatic mesogen to cross an aliphatic layer of a smectic or a cybotactic nematic. For a dimer this barrier would be $2E_0^*$, but for a polymer it would be $DP{\times}E_0^*$, where DP is the degree of polymerization. Such a high barrier would favour a smectic or a crystal phase over N_{tb}. We propose that the dimethylene spacer within the mesogen in our polymers reduces E_0^*, thus favouring longitudinal motion and stabilizing the N_{tb} phase.

Summary

BPE copolymers were revisited and re-characterised by GIXRD, polarised microscopy; polarised IR and modulated DSC. Analysis of vibrational modes revealed that the mesogens and oligomethylene spacers curve around the helical axis at similar angles. This suggests that the conformational average of the polymer chains is that of a helix, in agreement with models proposed for bent LC dimers.[9,12] Similar to previous work on the BPE-type copolymers[2] a four-point WAXS pattern was observed, arising from the tilt of the mesogens in respect to the helical axis. The average tilt angle and the order parameter of the helical axis were determined from the WAXS azimuthal distribution through deconvolution. Loss of the four point WAXS pattern and the jump in sample birefringence on transition to the N phase is believed to arise from straightening of the chain conformation. Azimuthal spreading of the WAXS arcs and decreased birefringence at the N-N_{tb} transition have both been reported also in systems of bent LC dimers. All experimental evidence indicates that the N-N transition is of the same nature in both the copolyethers and low MW LCs, dimers in particular. However, unlike other low MW LCs, the slow heating rate in MDSC experiments was found to broaden rather than sharpen the transition endotherms, an effect tentatively attributed to molecular weight segregation.

1. G. Ungar, J. L. Feijoo, A. Keller, R. Yourd, V. Percec, *Macromolecules*, 1990, **23**, 3411.
2. G. Ungar, V. Percec, M. Zuber, *Macromolecules*, 1992, **25**, 75.
3. G. Ungar, V. Percec, M. Zuber, *Polym. Bull.*, 1994, **32**, 1325.
4. D. Chen, M. Nakata, R. Shao, M. R. Tuchband, M. Shuai, U. Baumeister, W. Weissflog, D. M. Walba, M. A. Glaser, J. E. Maclennan, N. A. Clarke, *Phys. Rev. E*, 2014, **89**, 022506.
5. S. M. Jansze, A. Martínez-Felipe, J. D. M. Storey, A. T. M. Marcelis, C. T. Imrie, *Angew. Chem. Int. Ed.*, 2015, **54**, 643.
6. Y. Wang, G. Singh, D. M. Agra-Kooijman, M. Gao, H. K. Bisoyi, C. Xue, M. R. Fisch, S. Kumar, Q. Li, *CrystEngComm*, 2015, **1**, 2778.
7. A. Martínez-Felipe, C. T. Imrie, *J. Mol. Struct.*, 2015, **1100**, 429.
8. D. A. Paterson, A. Martinez-Felipe, S. M. Jansze, A. T. M. Marcelis, J. M. D. Storey, C. T. Imrie, *Liq. Cryst.*, 2015, **42**, 928.
9. R. J. Mandle, J. W. Goodby, *ChemPhysChem*, 2016, **17**, 967.
10. F. P. Simpson, R. J. Mandle, J. N. Moore, J. W. Goodby, *J. Mater. Chem. C*, 2017, **5**, 5102.
11. C. Zhu, M. R. Tuchband, A. Young, M. Shuai, A. Scarbrough, D. M. Walba, J. E. Maclennan, C. Wang, A. Hexemer, N. A. Clark, *PRL*, 2016, **116**, 147803.
12. W. D. Stevenson, Z. Ahmed, X. B. Zeng, C. Welch, G. Ungar, G. H. Mehl, *Phys. Chem. Chem. Phys.*, 2017, **19**, 13449.
13. M. Salamończyk, N. Vaupotič, D. Pociecha, C. Wang, C. Zhu, E. Gorecka, *Soft Matter*, 2017, **13**, 6694
14. K. Adlem, M. Čopič, G. R. Luckhurst, A. Mertelj, O. Parri, R. M. Richardson, B. D. Snow, B. A. Timimi, R. P. Tuffin, D. Wilkes. *Phys. Rev. E*, 2013, **88**, 022503.
15. L. Beguin, J. W. Emsley, M. Lelli, A. Lesage, G. R. Luckhurst, B. A. Timimi, H. Zimmermann, *J. Phys. Chem. B*, 2012, **116**, 7940.
16. A. Hoffmann, A. G. Vanakaras, A. Kohlmeier, G. H. Mehl, D. J. Photinos, *Soft Matter*, 2015, **11**, 850.
17. C. Meyer, G. R. Luckhurst, I. Dozov, *J. Mater. Chem. C*, 2015, **3**, 318.
18. V. P. Panov, M. Nagaraj, J. K. Vij, Y. P. Panarin, A. Kohlmeier, M. G. Tamba, R. A. Lewis, G. H. Mehl, *PRL.*, 2010, **105**, 167801.
19. C. Meyer, G. R. Luckhurst, I. Dozov, *Phys. Rev. Lett.*, 2013, **111**, 067801.
20. V. P. Panov, R. Balachandran, M. Nagaraj, J. K. Vij, M. G. Tamba, A. Kohlmeier, G. H. Mehl, *App. Phys. Lett.*, 2011, **99**, 261903.
21. E. Gorecka, M. Salamończyk, A. Zep, D. Pociecha, C.Welch, Z. Ahmed, G. H. Mehl, *Liq. Cryst.*, 2015, **42**, 1.
22. D. Chen, J. H. Porada, J. B. Hooper, A. Klittnick, Y. Shen, M. R.Tuchband, E. Korblova, D. Bedrov, D. M.Walba, M. A. Glaser, J. E. Maclennan, and N. A. Clark, *Proc. Natl. Acad. Sci. U.S.A.*, 2013, **110**, 15931.
23. V. Borshch, Y.-K. Kim, J. Xiang, M. Gao, A. J´akli, V. P. Panov, J. K. Vij, C. T. Imrie, M. G. Tamba, G. H. Mehl, O. D. Lavrentovich, *Nat. Commun.*, 2013, **4**, 2635.
24. P. K. Challa, V. Borshch, O. Parri, C. T. Imrie, S. N. Sprunt, J. T. Gleeson, O. D. Lavrentovich, A. Jákli, *Phys. Rev. E*, 2014, **89**, 060501.
25. M. Cestari, S. Diez-Berart, D. A. Dunmur, A. Ferrarini, M. R. de la Fuente, D. J. B. Jackson, D. O. Lopez, G. R. Luckhurst, M. A. Perez-Jubindo, R. M. Richardson, J. Salud, B. A. Timimi, and H. Zimmermann, *Phys. Rev. E*, 2011, **84**, 031704.
26. N. Sebastián, M. G. Tamba, R. Stannarius, M. R. de la Fuente, M. Salamończyk, G. Cukrov, J. Gleeson,

S. Sprunt, A. Jákli, C. Welch, Z. Ahmed, G. H. Mehl, A. Eremin, *Phys. Chem. Chem. Phys.*, 2016, **18**, 19299.

27. S. M. Salili, C. Kim, S. Sprunt, J. T. Gleeson, O. Parri, A. Jákli, *RSC Adv.*, 2014, **4**, 57423.

28. P. A. Henderson, C. T. Imrie, *Liq. Cryst.*, 2011, **38**, 1407.

29. V. Percec, R. Yourd, *Macromolecules*, 1988, **21**, 3379.

30. R. J. Mandle, *Soft Matter*, 2016, **12**, 7883.

31. R. J. Mandle, *Chem. Eur. J.*, 2016, **22**, 18456.

32. A. M. Donald, A. H. Windle (1992). "*Liquid Crystalline Polymers*", Cambridge University Press, pp. 223-224.

33. A. J. Guenthner, T. Kyu, *Macromolecules*, 2000, **33**, 4463.

34. G. Ungar, in "*Physical Properties of Liquid Crystals: Nematics*", eds. DA Dunmur, A Fukuda, GR Luckhurst, IEEE (Inspec), London, 2000, "*X-ray Studies of Nematic Systems*", pp. 177-192.

35. Z. Zhang, V. P. Panov, M. Nagaraj, R. J. Mandle, J. W. Goodby, G. R. Luckhurst, J. C. Jones, H. F. Gleeson, *J. Mater. Chem. C*, 2015, **3**, 10007.

36. D. M. Agra-Kooijman, G. Singh, M. R. Fisch, M. R. Vengatesan, J.-K. Song, S. Kumar, *Liq. Cryst.*, 2017, **44**, 191.

37. J. P. Jokisaari, G. R. Luckhurst, B. A. Timmi, J. Zhu, H. Zimmermann, *Liq. Cryst.*, 2015, **42**, 708.

38. C.-P. Lafrance, A. Nabet, R. E. Prud'homme, M. Pézolet, *Can. J. Chem.*, 1995, **73**, 1497.

39. R. L. Silvestri, J. L. Koenig, *Polymer*, 1994, **35**, 2528.

40. W.-S. Park, *J. Korean Phys. Soc.*, 2000, **37**, 331.

41. C. T. Archbold, R. J. Mandle, J. L. Andrews, S. J. Cowling, J. W. Goodby, *Liq. Cryst.*, 2017, **44**, 2079.

42. M. B. Sied, J. Salud, D. O. Lopez, M. Barrio, J. L. Tamarit, *Phys. Chem. Chem. Phys.*, 2002, **4**, 2587.

43. I. Hatta, S. Muramatsu, *Jpn. J. Appl. Phys.* 1996, **35** L858.

44. W. D. Stevenson, H. X. Zou, C. Welch, X. B. Zeng, G. H. Mehl, G. Ungar, in preparation.

45. C. A. Croxton, *Macromolecules*, 1991, **24**, 537.